Computational Analysis of Horizontal Axis Wind Turbine Blade NACA 63(4)221

Uma MaheshwarVanamala*, PurnaVisishtaBattu

*Department of Mechanical Engineering
University College of Engineering, Osmania University
Hyderabad, Telangana, 500007

Abstract

Wind energy is one of the most sustainable sources of renewable energy. The fast technological development in the wind industry and availability of multi megawatt sized horizontal axis wind turbines has further led to the promotion of wind power utilization globally. The paper presents work on NACA 63(4)-221 aerofoilprofile is taken which is redesigned horizontal axis wind turbine blade (HAWT) for VESTAS RRB V27-225 kW. In a HAWT, aerofoil blades are very essential parts. Forces for lift and drag on the blade play an important role in the aerodynamic efficiency of aerofoil. CFD analysis on the aerofoil blade of wind turbine is carried out and the effect of angle of attack and Reynolds number on performance of the NACA 63(4)-221 aerofoilblade is presented. The ratio of coefficient of lift to coefficient of drag (C_l/C_d) is calculated. Maximum C_l/C_d values are observed at Angle of Attack 6^o degrees.

Keywords: *Horizontal Axis Wind Turbine, Aerofoil, Angle of Attack, Reynolds number.*

1. Introduction

A wind turbine, or alternatively referred to as a wind energy converter, is a device that converts the wind's kinetic energy into electrical energy. Wind energy is a form of solar energy. Wind is caused by the uneven heating of the earth’s atmosphere by the solar radiation, variations in the earth's surface, and rotation of the earth. So the energy is from the Sun.

A Wind turbine uses the wind’s kinetic energy and converts it into mechanical energy, that is, rotations the blades of the wind turbine. The blades spin a shaft that is connected through a gearbox to the generator which produces electricity, in conventional wind turbines. The most recognizable parts of a turbine are its blades. Many turbines today have three blades, while some have two. Atmospheric turbulence (unsteady movement of air) produces important various types of aerodynamic forces (lift and drag) on wind turbine blade, where turbulence is a primary source of aerodynamic forces on blade of wind turbine.

2. Literature Review

A lot of work and studies have been done on turbines blades which are described in various research papers. Few of the papers which are referred are described below.

H. Abbott, Albert E. Yondoenhoff and Louis S. Stiyers (1945); in National Advisory Committee for Aeronautics, Report No. 824, Summary of Aerofoil Data, have collected aerofoil data for both flight and wind-tunnel tests and correlated. They found that the NACA 6-series aerofoils also have favourable critical-speed characteristics and do not appear to present unusual problems associated with the application of high-lift and lateral-control devices.UmeshChaudhary; Sisir Kumar Nayak (2015); “Micro and small-scale HAWT blades aerofoils study through CFD for low wind applications” analysis of basic 5 series NACA aerofoils profile for micro and small-scale horizontal axis wind turbine (HAWT) has been

*Corresponding author: E-mail: Mahesh.v@uceou.edu

studied for different angle-of-attack α and fixed Reynolds number and found the optimal angle-of-attack.

MingweiGe,; De Tian,; and Ying Deng (2016); "Reynolds Number Effect on the Optimization of a Wind Turbine Blade for Maximum Aerodynamic Efficiency" have investigated the effect of the Reynolds number on the aerodynamic performance of aerofoils, and influence on the optimal design of a wind rotor aiming to maximize the power coefficient.GiridharRamanujam, HüseyinÖzdemir and H. W. M. Hoeijmakers (2016); in "Improving Aerofoil Drag Prediction" have developed an improved formulation of drag estimation for thick aerofoils. The improved drag formulation predicts the drag accurately for aerofoils with reasonably small trailing-edge thicknesses. The derivation of drag correction is based on the difference between the actual momentum loss thickness based on free stream velocity and that based on the velocity at the edge of the boundary layer. A modification to the existing drag calculation method till then in XFOIL-like methods has been developed.

C.A. Baxevanoua, P.K. Chaviaropoulosb, S.G. Voutsinas c, N.S. Vlachosa (2008); "Evaluation study of a Navier–Stokes CFD aero elastic model of wind turbine aerofoils in classical flutter" described a new aero elastic numerical model, which combines a Navier–Stokes CFD solver with an elastic model and two coupling schemes for the study of the aero elastic behaviour of wind turbine blades undergoing classical flutter. There model is evaluated by comparing with previous numerical results and the corresponding linear analytical solutions. Consequently, a parametric study is carried out. Conclusions are drawn about the ability of the model to handle the aero elastic behaviour of an aerofoil and about the most appropriate coupling scheme in terms of predicting the modal damping and the flutter limiting point. There predictions show that they are only slightly affected by the coupling or the space discretization scheme and mainly by the turbulence model used.

Muhammad FaizanYounas, Awais Ali and Muhammad DaudShafique(2019);" CFD Simulation of HAWT Blade and Implementation of BEM Theory"; designed HAWT implemented Blade Element Momentum Theory (BEM), studied the characteristics of flow over the designed blade in Computational Fluid Dynamics (CFD) and simulations where done using ANSYS Fluent.In present work CFD analysis for airfoil NACA 63(4)-221 for redesigning the blade of VESTAS RRB V27-225 kW Horizontal Axis Wind Turbine (HAWT). In this work the viscous SpalartAllmaras model is used. SpalartAllmaras model is a one equation model which solves a transport equation for a viscosity-like variable, referred to as the Spalart-Allmaras variable.

3. PROBLEM DEFINITION

NACA series blades have been experimented in a wind tunnel and the results were obtained. Computationally the analysis can be done on the blades of the turbine so as to predict the performance before it is experimented and been installed for applications. This can help for better performance, eliminate deficient conditions, reduce time and cost.

3.1 OBJECTIVES

The horizontal axis wind turbine blade for VESTAS RRB V27-225 kW, computational study on the performance of an aerofoil blade profile NACA 63(4)-221 is carried out with the following objectives.

i. To conduct analysis on Horizontal axis wind turbine blade NACA 63(4)221 profile.

ii. To determine lift coefficient (C_l), drag coefficient (C_d), ratio of lift coefficient to drag coefficient (C_l/C_d) of the aerofoil.

iii. To determine angle of attack where C_l/C_d is maximum.

The following flow Parameters are varied in the study:

a) Angle of Attack: 4^0, 5^0, 6^0, 7^0, 8^0.

b) Low Reynolds number in the range of $X10^5$ (wind speed: 6 m/s, 7 m/s, 8 m/s, 9 m/s, 10 m/s).

c) High Reynolds number in the range of $X10^6$ (wind speed: 43.8 m/s, 87.6 m/s, 131.5 m/s).

4. RESEARCH METHODOLOGY

4.1. MODELING GEOMETRY

The coordinates of the NACA 634-221 are obtained from literature P. K. Nigam (2020) [7]. The aerofoil is designed by selecting required coordinate file in the Design modeller. A rectangular domain is designed using sketching tool for analysis around the aerofoil. Then the required design is obtained using Boolean operation. Figure 1 shows the designed aerofoil profile of NACA 634-221. The boundary conditions which are defined in setup are been named using named selections of the aerofoil: inlet, outlet, top, bottom, aerofoil top, aerofoil bottom and 2d design profile.

4.2. MESH

Mesh is done around the aerofoil with physics preference CFD and Solver preference is Fluent. Edge sizing of the aerofoil cross-section is done, in inflation the boundary as the aerofoil edges is selected for obtaining finer mesh around the aerofoil. The mesh is generated in ANSYS Workbench 2020 R2 by using ANSYS Fluent 2020 R2, is shown in the figure 2.

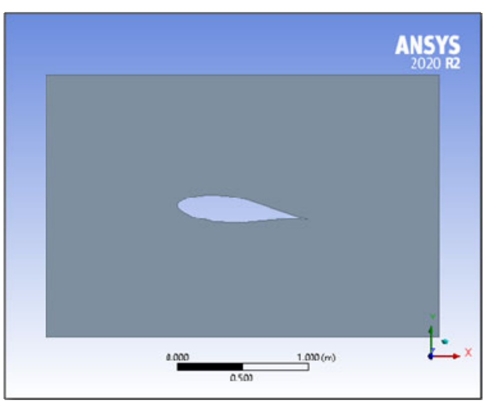

Figure 1: NACA 63_4-221aerofoil profile

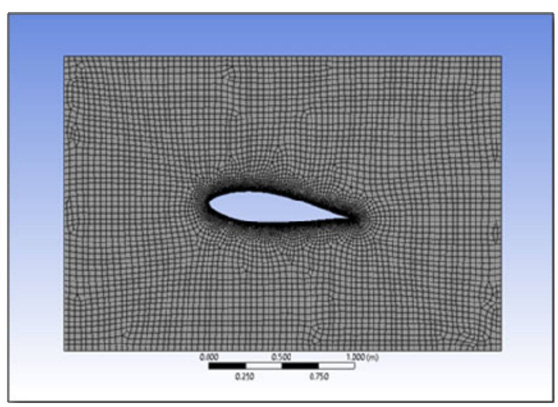

Figure 2: Mesh around NACA 63_4-221

4.3. GRID INDEPENDENCE STUDY

A solution is considered grid-independent if the discretization and solution error are small enough, given sufficient iterations. This is essential to know for comparative results. A mesh convergence study consists of refining elements and comparing the refined solutions to the

ISBN - 978-93-95038-50-8

coarse solutions. If further refinement (or other changes) does not significantly change the solution, the mesh is an "Independent Grid."

In this analysis, mesh is performed at angle of attack=60, inlet velocity: 6m/s for the aerofoil. When the increase in the change in Cl/Cd coefficient becomes negligible, the optimum mesh number is determined. Table 1 shows the grid independence test results.

From these results, of the grid independence test, mesh is determined at 17866 nodes and 17264 elements for best results.

Element size: 0.04m (linear element order)

Number of divisions (aerofoil edges): 500(Behaviour: Hard)

Inflation between face and edges of aerofoil: 8 layers with 0.01 maximum thickness

In meshing finer mesh is done around the aerofoil to obtain accurate values of Lift and Drag coefficient around the aerofoil

Table 1: Grid Independence Test Results

NODES	**Cl/Cd**
13838	74.40807477
15099	74.04116318
15488	74.42551651
16009	74.84930386
16512	74.49607027
17866	**75.21509212**
18787	75.1802723
19313	74.63732116
20526	74.84930386

The geometry is designed at varies angle of attack and is been meshed accordingly after the grid independence test. The Table 2 shows the number of nodes obtained at different angle of attack.

Table 2: Mesh size at Angle of Attack

Angle of Attack	**Nodes**
4^0	17794
5^0	17810
6^0	17866
7^0	17911
8^0	17983

4.4. Validation

At the end of each analysis, the ratio Cl/Cd for a given angle of attack were calculated, compared and validated with the results available in the literature P. K. Nigam (2020) and Abbott I.H (1945).

Case1: At low Reynolds Number, inlet velocity=6 m/s for the aerofoil. The values of Cl/Cd are calculated, compared and validated with the results available in the literature P. K. Nigam (2020) [7]. Table 3 shows the validation results at varying angle of attack at low Reynolds number.

Table 3: Validation at low Reynolds number

Angle of Attack(AOA)	**C_l/C_d**	**Reference C_l/C_d [7]**
4^o	67.820	70.847
5^o	73.061	75.814
6^o	75.215	78.457
7^o	73.731	78.017
8^o	70.932	74.662

Case2: At high Reynolds Number, inlet velocity= 43.8 m/s (Re=3x106) for the aerofoil. The values of Cl/Cd are calculated, compared and validated with the results available in the literature Abbott I.H (1945) [1] and P. K. Nigam (2020) [7].Table 4 shows the validation results at varying angle of attack at high Reynolds number.

Table 4: Validation at high Reynolds number

Angle of Attack(AOA)	**C_l/C_d**	**Reference C_l/C_d [1]**	**Reference C_l/C_d[7]**
4^o	96.232	0.55/0.0067=82.089	-
5^o	102.183	0.77/0.0072=106.944	108.854
6^o	105.724	0.86/0.0079=108.861	111.613
7^o	104.085	0.975/0.009=108.333	111.120
8^o	102.970	1.05/0.0114=92.110	108.280

4.5 SETUP

4.5.1BOUNDARY CONDITIONS

The analysis consists of flow around an aerofoil at various angles of attack (4^o, 5^o, 6^o, 7^o, 8^o) and at different Reynolds number in the range of 10^5 and 10^6.

Reynolds Number (Re): The Reynolds number is a dimensionless number used to predict flow patterns in different fluid flow situations. The ratio of inertial forces to viscous forces gives Reynolds number.

$$Re = \frac{Inertial\ Force}{Viscous\ Force} = \frac{\rho v l}{\mu} = \frac{vl}{\vartheta}$$

Where, ρ is the density of the fluid (kg/m3)

v is the wind speed (m/s)

l is a characteristic linear dimension (m) μ is the dynamic viscosity of the fluid (Pa·s) or N·s/m2 or kg/(m·s)

ϑ is the kinematic viscosity of the fluid (m2/s)

From the above equation of Reynolds number, wind velocity is calculated for high values of Reynolds number: 3x106, 6x106, 9 x 106.

$$Wind\ Speed\ \mathrm{v} = \frac{Re\ \mu}{\rho l}$$

Calculations of wind velocities at high Reynolds number:

Here air is the medium so; ρ=1.225 m/s, μ= 1.7894×10^{-5} kg/m-s and chord length l=1m

At $Re=3x10^6$ $\quad V = \frac{3x10^6 x1.7894x10^{-5}}{1.225x1}$ =43.822 m/s

At $Re=6x10^6$ $\quad V = \frac{6x10^6 x1.7894x10^{-5}}{1.225x1}$ =87.644m/s

At $Re=9x10^6$ $\quad V = \frac{9x10^6 x1.7894x10^{-5}}{1.225x1}$ =131.466 m/s

Energy equation and Viscous Spalart-Allmaras(1 Equation) model is been used for the calculation. The Spalart-Allmaras model is a relatively simple one-equation model that solves a modelled transport equation for the kinematic eddy (turbulent) viscosity. The inputs and boundary conditions are shown in the Table 5.

Table 5: The parameters considered in the Fluent Setup

Fluent Setup	
Physics Preference	CFD
Solver Preference	Fluent
Problem Type	2D
Type of Solver	Pressure-Based Solver
Models	
Energy Equation	On
Viscous Model	SpalartAllmaras(1 Equation)
Material Properties	Flowing fluid is air
Density of air	1.225 kg/m^3
Viscosity	$1.7894e^{-05}$ kg/m-s
Boundary Conditions	
Velocity Inlet	
Velocity(m/s)	6, 7, 8, 9, 10, 43.8, 87.6, 131.5
Pressure outlet	
Gauge pressure	0 Pa
Turbulent viscous ratio	10

5. SOLUTION METHOD

Table 6 shows solver conditions for obtaining the calculated results of lift coefficient and drag coefficient. The required solutions which are to be calculated are been defined in report definitions to graphically plot and view results. The calculations are done by running with 200 iterations for all parameters varying for the solutions to converge.

Table 6: Solution Method

Solution Method	
Pressure velocity coupling	
Scheme	Coupled
Spatial Discretization	
Gradient	Least Squares Cell Based
Pressure	Second Order
Momentum	Second Order Upwind
Modified turbulent	First Order Upwind
Energy	Second Order Upwind
Report Definitions	
Report File and Report	Lift coefficient, Drag
Solution Initialization	
Initialization Method	Hybrid Initialization
Run Calculations	
Number of iterations	200

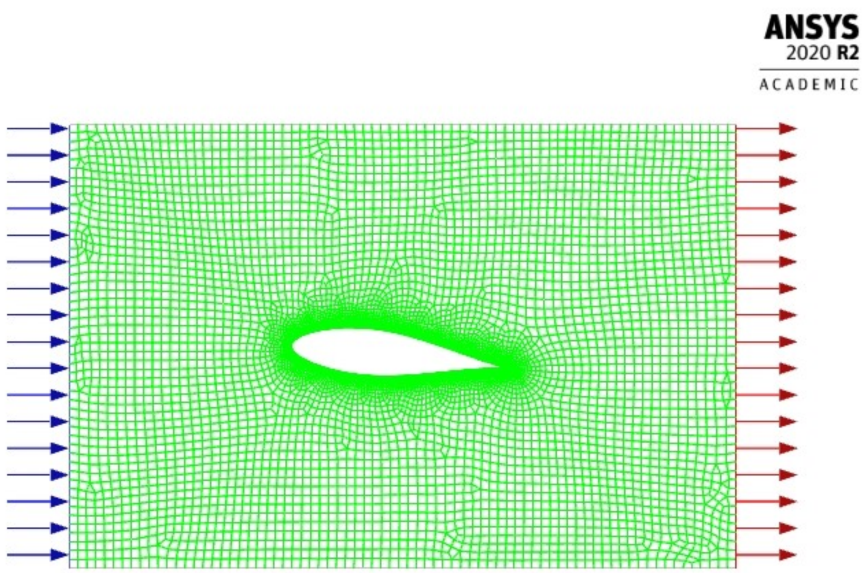

Figure 3: NACA 63_4-221 with inlet and outlet

5. RESULTS AND DISCUSSIONS

From these contours obtained it is observed that they are lower values of pressure on the top of the aerofoil, higher values of pressure on the bottom of the aerofoil, likewise, higher values of velocity on the top of the aerofoil, lower values of velocity on the bottom of the aerofoil. So there is a significant amount of lift on the top of the aerofoil.

Figures 4 to 19 shows the velocity distribution and pressure distribution around aerofoil at Angle of attack=6° at velocities=6m/s, 7m/s, 8m/s, 9m/s, 10m/s, 43.8m/s, 87.6m/s and 131.5m/s.

At a particular angle of attack, as the wind velocity increases there is increase in velocity of the aerofoil. It is also observed that as the angle of attack increases there is an increase in velocity of the aerofoil.

From the velocity contours the following are the observations:

a) As the wind velocity is increased the velocity around the aerofoil is increasing.
b) The velocity is higher on the top of the aerofoil compared to the bottom of the aerofoil.
c) The maximum values of velocity are on the top of the aerofoil.
d) The minimum values of velocity are at the leading edge and trailing edge of the aerofoil.

From the static pressure contours the following are the observations:

a) As the wind velocity is increased the static pressure around the aerofoil is increasing.
b) The pressure is lower on the top of the aerofoil compared to the bottom of the aerofoil.
c) The maximum values of static pressure are at the leading edge the aerofoil.

In viewpoint on effect of AOA on velocity contours and pressure contours, it is observed that with the increase in angle of attack from 4º to 8º

i. The velocity around the aerofoil is increasing.
ii. The range of velocity distribution around the aerofoil is increasing.
iii. The static pressure around the aerofoil is increasing.
iv. The range of static pressure distribution around the aerofoil is increasing.

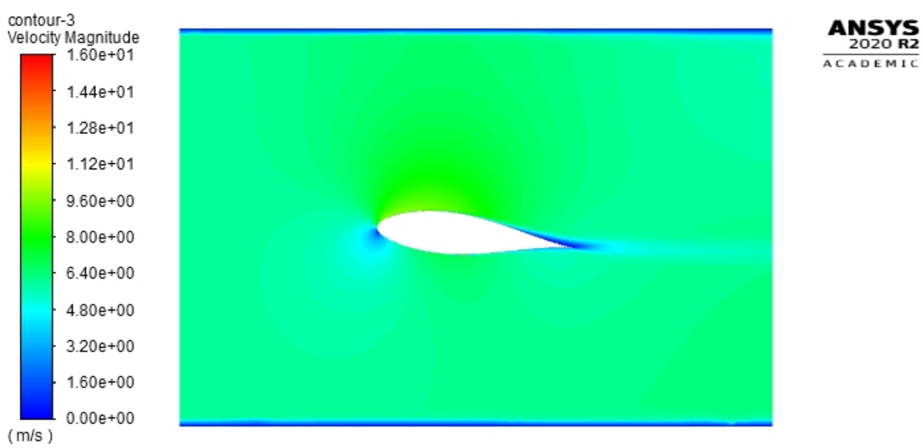

Figure 4: Velocity distribution around Aerofoil-NACA 63(4)-221 at AOA=6° and v=6 m/s

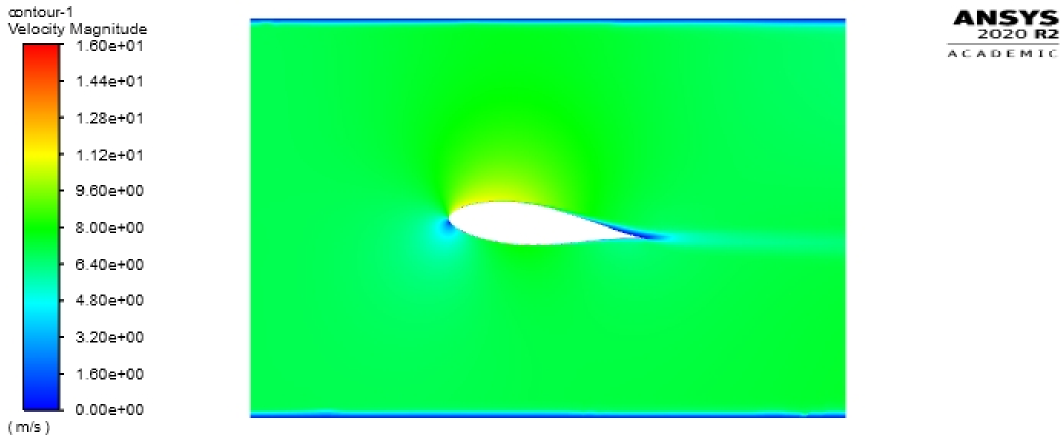

Figure 5: Velocity distribution around Aerofoil-NACA 63(4)-221 at AOA=6° and v=7 m/s

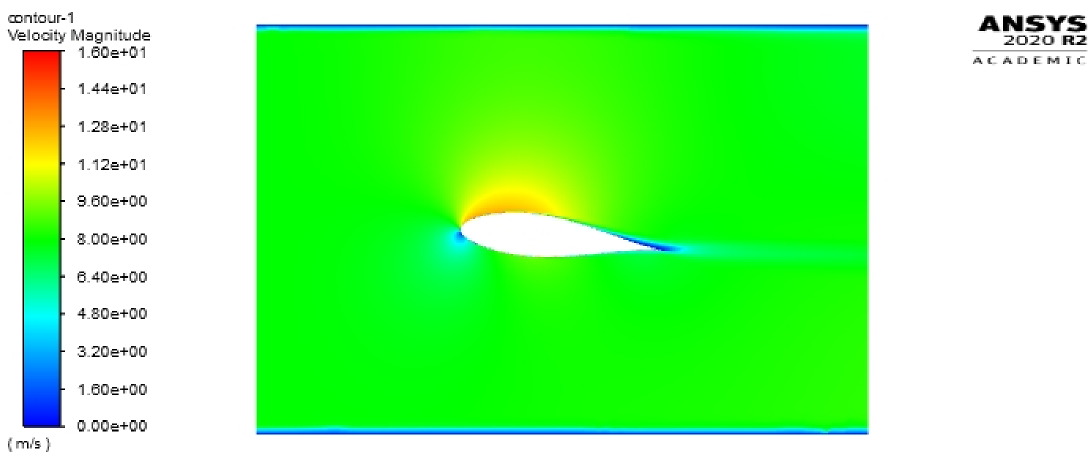

Figure 6: Velocity distribution around Aerofoil-NACA 63(4)-221 at AOA=6° and v=8 m/s

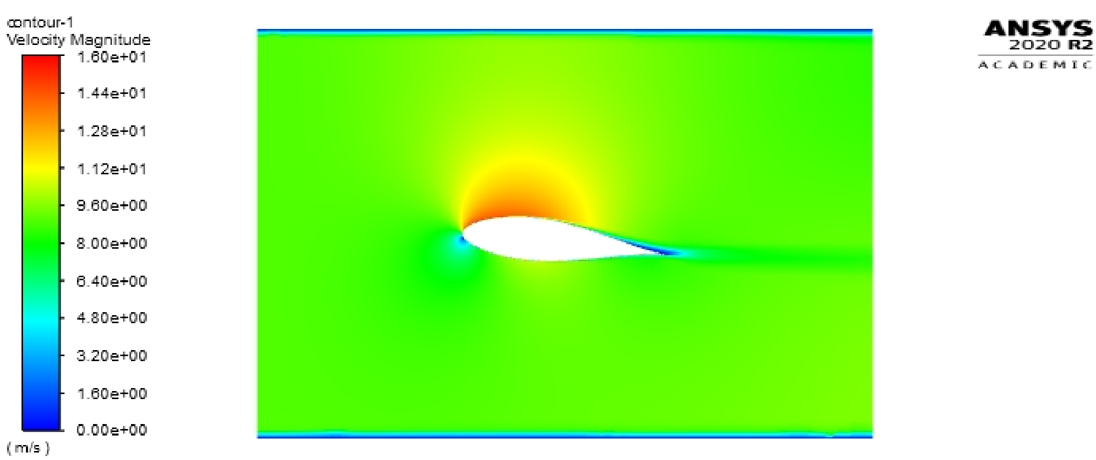

Figure 7: Velocity distribution around Aerofoil-NACA 63(4)-221 at AOA=6° and v=9 m/s

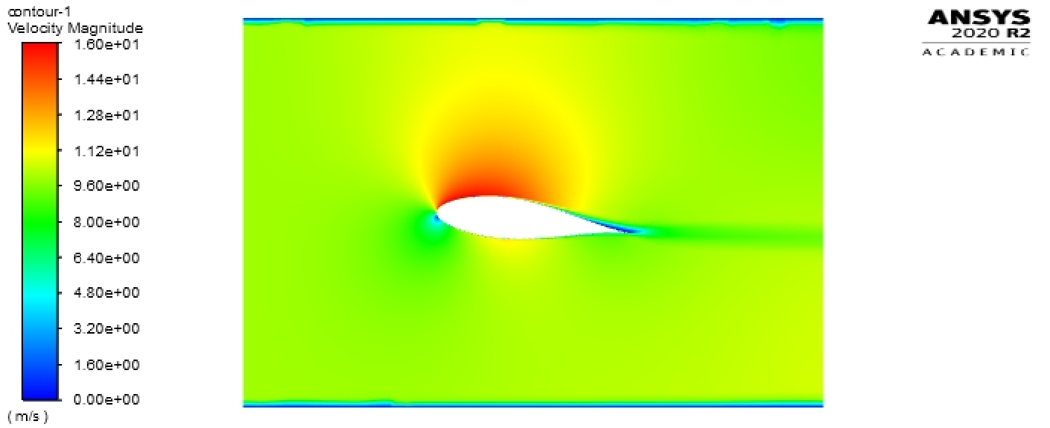

Figure 8: Velocity distribution around Aerofoil-NACA 63(4)-221 at AOA=6° and v=10 m/s

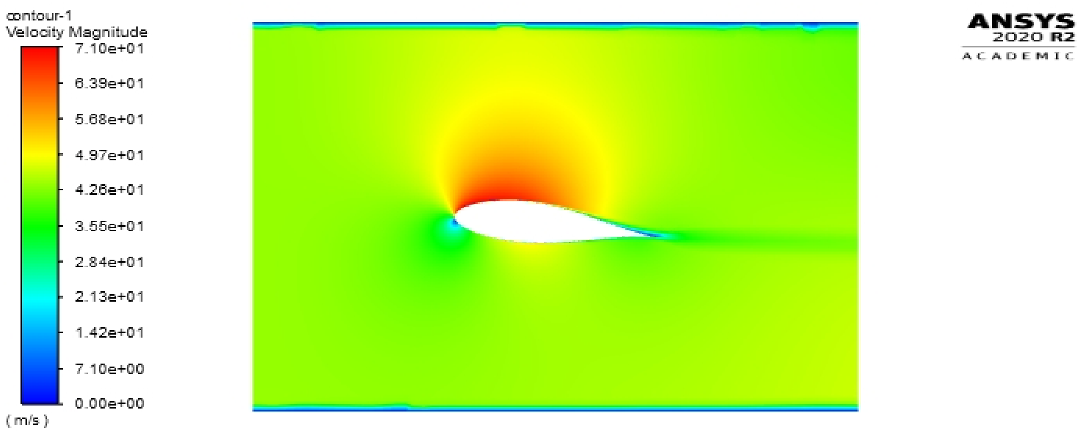

Figure 9: Velocity distribution around Aerofoil-NACA 63(4)-221 at AOA=6° and v=43.8 m/s

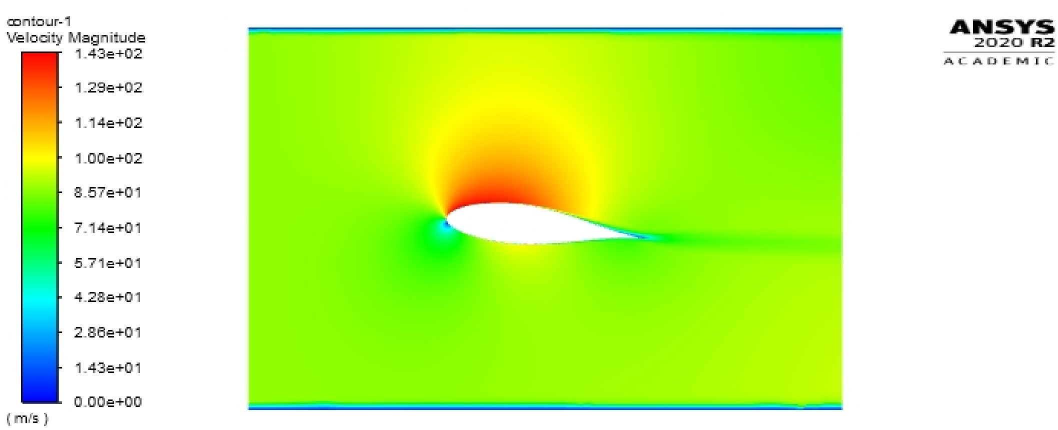

Figure 10: Velocity distribution around Aerofoil-NACA 63(4)-221 at AOA=6° and v=87.6 m /s

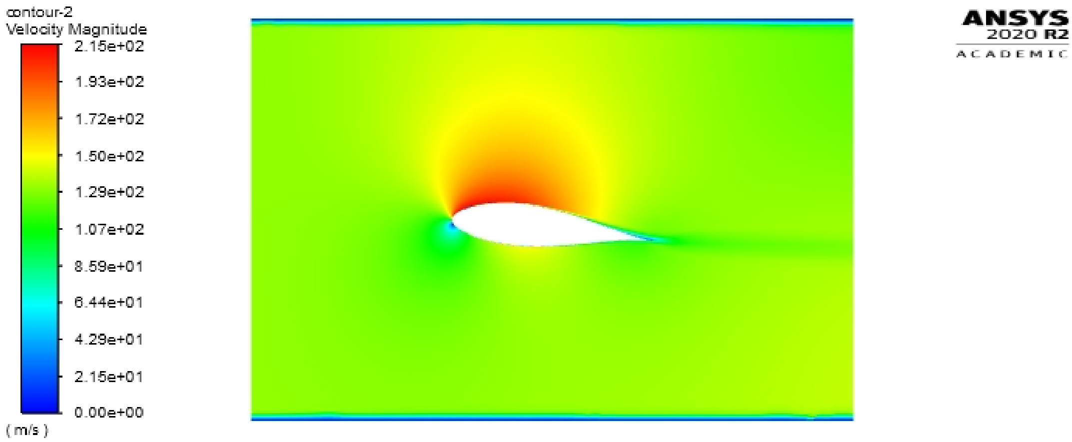

Figure 11: Velocity distribution around Aerofoil-NACA 63(4)-221 at AOA=6° and v=131.5 m /s

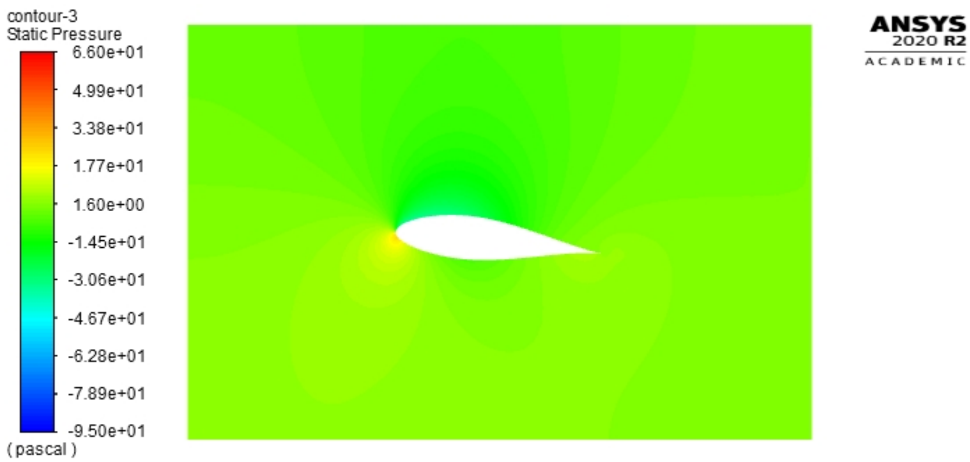

Figure 12: Static Pressure distribution around Aerofoil-NACA 63(4)-221 at AOA=6° and v=6 m/s

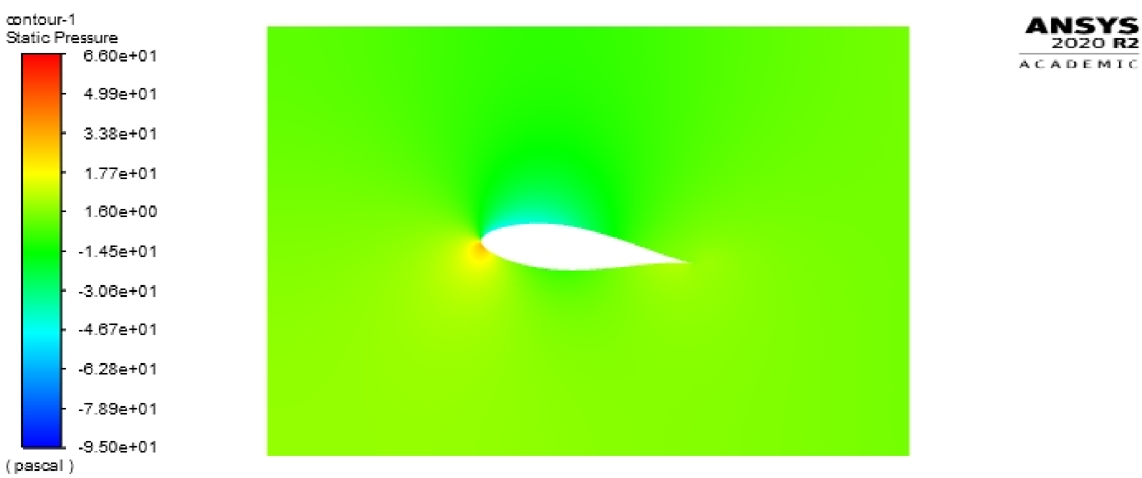

Figure 13: Static Pressure distribution around Aerofoil-NACA 63(4)-221 at AOA=6° and v=7 m/s

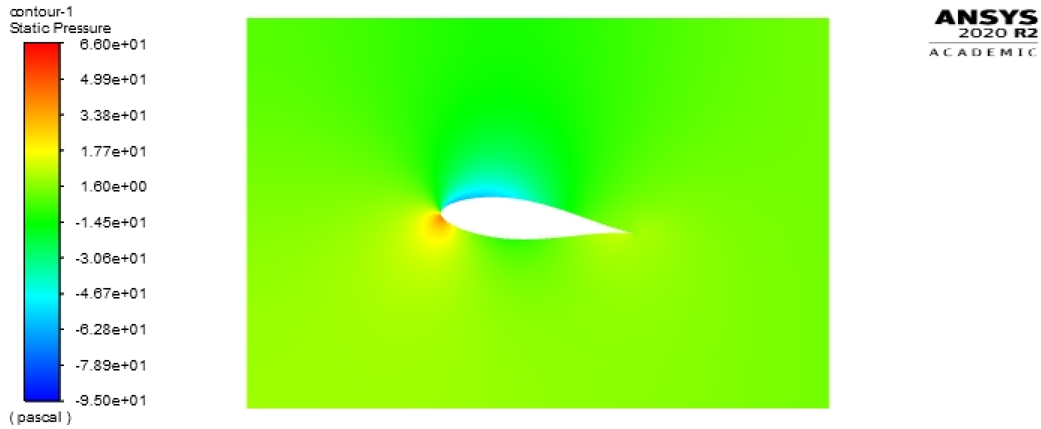

Figure 14: Static Pressure distribution around Aerofoil-NACA 63(4)-221 at AOA=6° and v=8 m/s

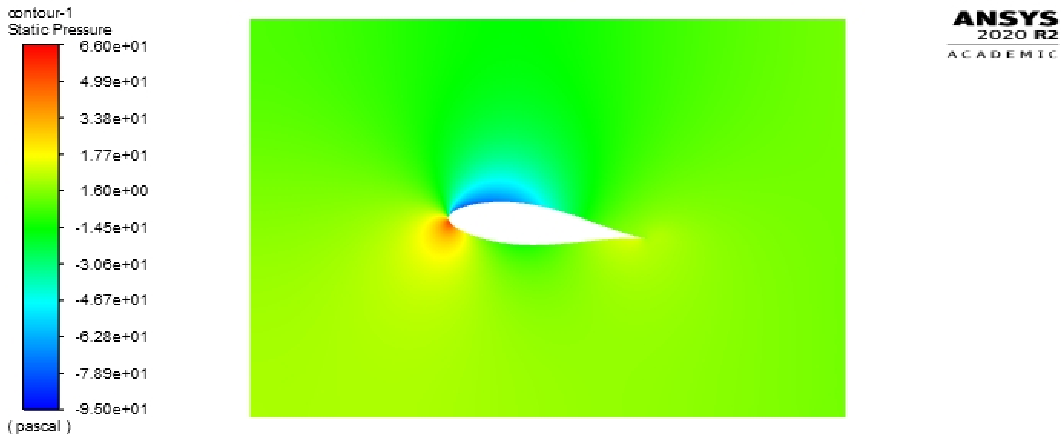

Figure 15: Static Pressure distribution around Aerofoil-NACA 63(4)-221 at AOA=6° and v=9 m/s

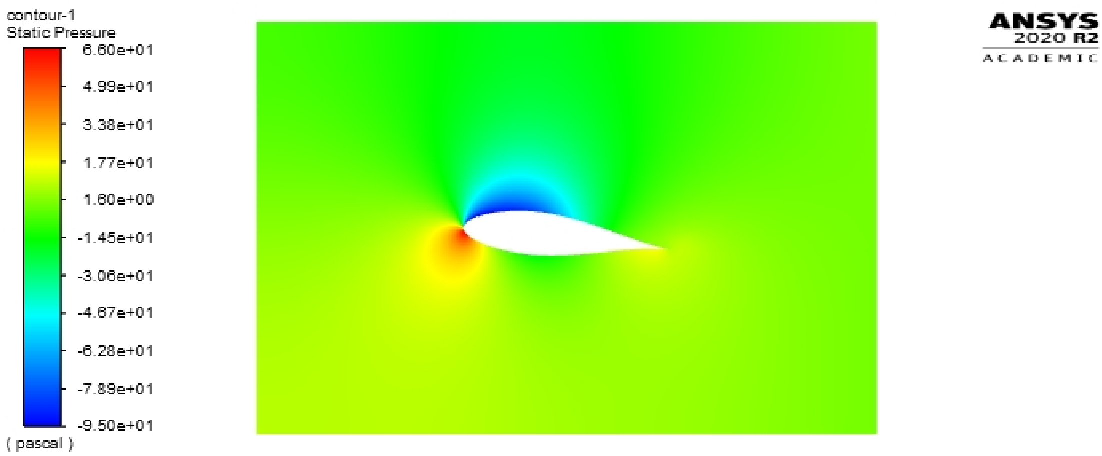

Figure 16: Static Pressure distribution around Aerofoil-NACA 63(4)-221 at AOA=6° and v=10 m/s

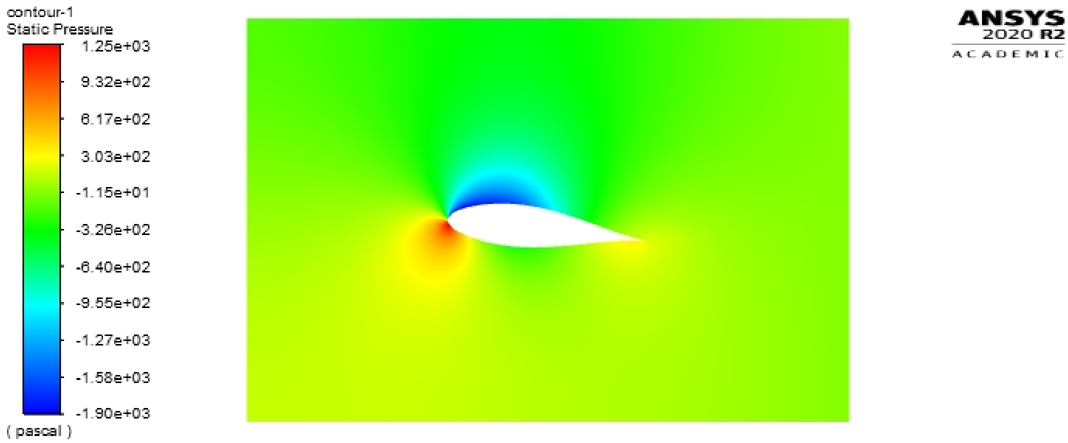

Figure 17: Static Pressure distribution around Aerofoil-NACA 63(4)-221 at AOA=6° and v=43.8 m/s

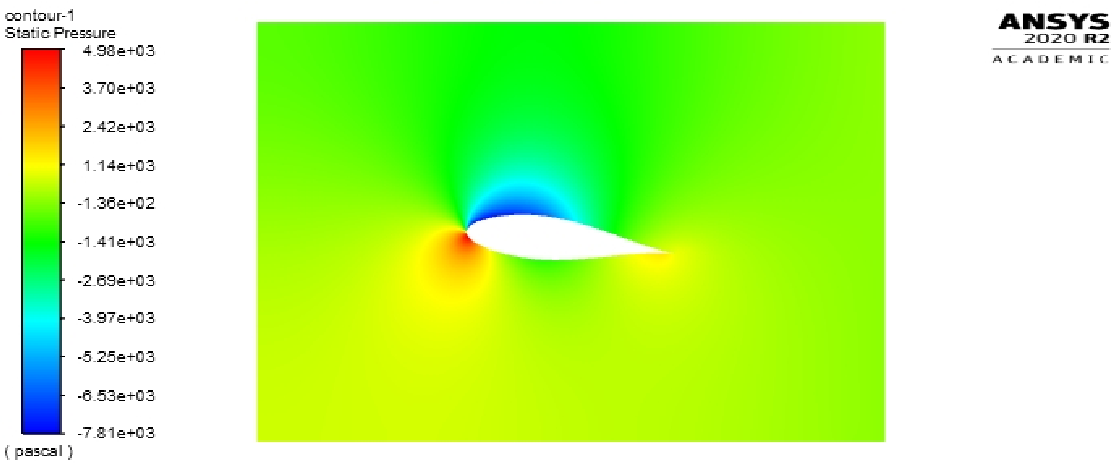

Figure 18: Static Pressure distribution around Aerofoil-NACA 63(4)-221 at AOA=6° and v=87.6m/s

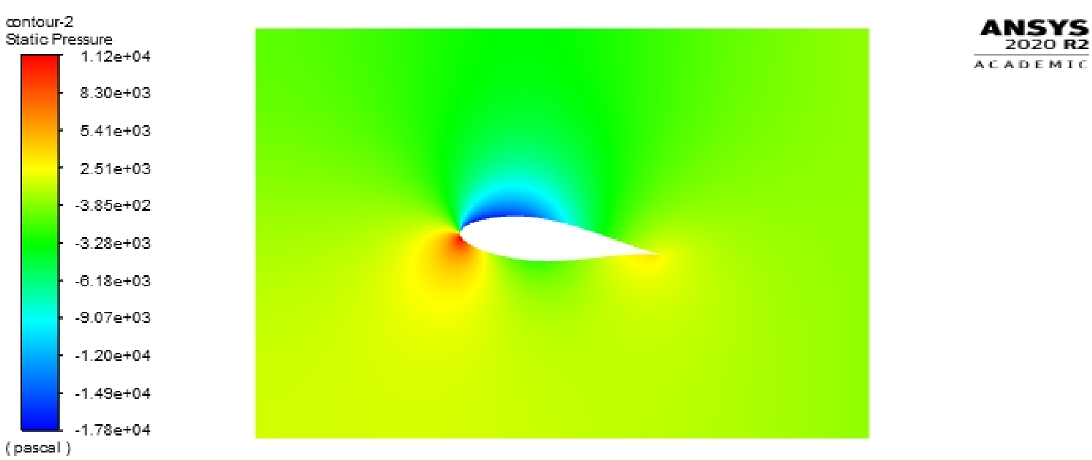

Figure 19: Static Pressure distribution around Aerofoil-NACA 63(4)-221 at AOA=6° and v=131.5 m/s

ISBN - 978-93-95038-50-8

Table 7 shows the calculated values of lift coefficient, drag coefficient at angle of attack 4° to 8° at low values of Reynolds number in CFD and figures 20, 22, 24 shows the graphs plotted from them. Table 8 shows the calculated values of lift coefficient, drag coefficient at angle of attack 4o to 8o at high values of Reynolds number in CFD and figures 21, 23, 25 shows the graphs plotted from them.

The improved drag formulation predicts the drag accurately for aerofoils with reasonably small trailing-edge thicknesses. The derivation of drag correction is based on the difference between the actual momentum loss thickness based on free stream velocity and that based on the velocity at the edge of the boundary layer. A correction factor 0.4 is multiplied to the obtained drag coefficient in CFD to get corrected drag coefficient as explained by GiridharRamanujam (2016) [5].

TABLE 7: CFD analysis results of NACA aerofoil 63(4)-221 at various angle of attack and wind speed for low Reynolds number (x 10^5)

Angle of Attack (degrees)	Reynolds Number	Wind Speed (m/s)	Coefficient of Lift C_l	Coefficient of Drag C_d^1	Corrected Coefficient of Drag $C_d = C_d^1 * 0.4$	C_l/C_d
4^0	410752.20	6	0.62389	0.022997	0.0091992	67.82
4^0	479210.90	7	0.62784	0.022318	0.0089274	70.32
4^0	547669.60	8	0.63086	0.021846	0.0087383	72.19
4^0	616128.31	9	0.63321	0.021493	0.0085972	73.65
4^0	684587.01	10	0.63538	0.021190	0.0084761	74.96
5^0	410752.20	6	0.74093	0.025353	0.0101412	73.06
5^0	479210.90	7	0.74608	0.024681	0.0098725	75.57
5^0	547669.60	8	0.74917	0.024208	0.0096834	77.36
5^0	616128.31	9	0.75160	0.023835	0.0095341	78.83
5^0	684587.01	10	0.75412	0.023501	0.0094006	80.22
6^0	410752.20	6	0.84433	0.028064	0.0112256	75.21
6^0	479210.90	7	0.85024	0.027361	0.0109445	77.68
6^0	547669.60	8	0.85374	0.026870	0.0107482	79.43
6^0	616128.31	9	0.85685	0.026463	0.0105853	80.94
6^0	684587.01	10	0.85999	0.026097	0.0104389	82.38
7^0	410752.20	6	0.94236	0.031952	0.0127810	73.73
7^0	479210.90	7	0.94921	0.031196	0.0124786	76.06
7^0	547669.60	8	0.95343	0.030661	0.0122645	77.73
7^0	616128.31	9	0.95740	0.030201	0.0120806	79.25
7^0	684587.01	10	0.96072	0.029826	0.0119305	80.52
8^0	410752.20	6	1.02121	0.035992	0.0143969	70.93
8^0	479210.90	7	1.02919	0.035177	0.0140709	73.14
8^0	547669.60	8	1.03484	0.034576	0.0138305	74.82
8^0	616128.31	9	1.03984	0.034047	0.0136190	76.35
8^0	684587.01	10	1.04370	0.033633	0.0134532	77.58

MAXIMUM C_l/C_D VALUES ARE OBSERVED AT ANGLE OF ATTACK=6 DEGREE

TABLE 8: CFD analysis results of NACA aerofoil 63(4)-221 at various angle of attack and wind speed for high Reynolds number (x10^6)

Angle of Attack (degrees)	Reynolds Number	Wind Speed (m/s)	Coefficient Of Lift C_l	Coefficient Of Drag C_d^1	Corrected Coefficient Of Drag $C_d=C_d^1*0.4$	C_l/C_d
4^0	3000000	43.8	0.46411	0.012057	0.0048228	96.23
4^0	6000000	87.6	0.45447	0.010459	0.0041837	108.62
4^0	9000000	131.5	0.45838	0.009966	0.0036447	114.98
5^0	3000000	43.8	0.78772	0.019272	0.0077089	102.18
5^0	6000000	87.6	0.80490	0.017807	0.0070229	113.00
5^0	9000000	131.5	0.81369	0.017088	0.0068355	119.04
6^0	3000000	43.8	0.90470	0.021393	0.0085572	105.72
6^0	6000000	87.6	0.92632	0.019884	0.0079535	116.46
6^0	9000000	131.5	0.93658	0.019089	0.0076358	122.65
7^0	3000000	43.8	1.02227	0.024554	0.0098216	104.08
7^0	6000000	87.6	1.04667	0.023060	0.0092241	113.47
7^0	9000000	131.5	1.05839	0.022230	0.0089210	119.02
8^0	3000000	43.8	1.12848	0.027398	0.0109593	102.97
8^0	6000000	87.6	1.16384	0.02562	0.0102470	113.58
8^0	9000000	131.5	1.17842	0.024892	0.0099569	118.35

MAXIMUM C_l/C_D VALUES ARE OBSERVED AT ANGLE OF ATTACK=6 DEGREES

Combined effect of AOA and Wind velocity on Lift Coefficient at low Reynolds number and high Reynolds number

Figure 20 and figure 21 shows the Lift Coefficient at different angle of attack for wind velocities at low Reynolds number and high Reynolds number respectively. The following are the observations from them:

a) The lift coefficient is increasing as the angle of attack is increased.
b) The lift coefficient is increasing as the wind velocity is increased.
c) The difference in increase in lift coefficient is identical as the wind velocity increases and angle of attack increases.
d) The difference in increase in lift coefficient at AOA 4^o to 5^o is more compared to other successive AOA at high Reynolds number.

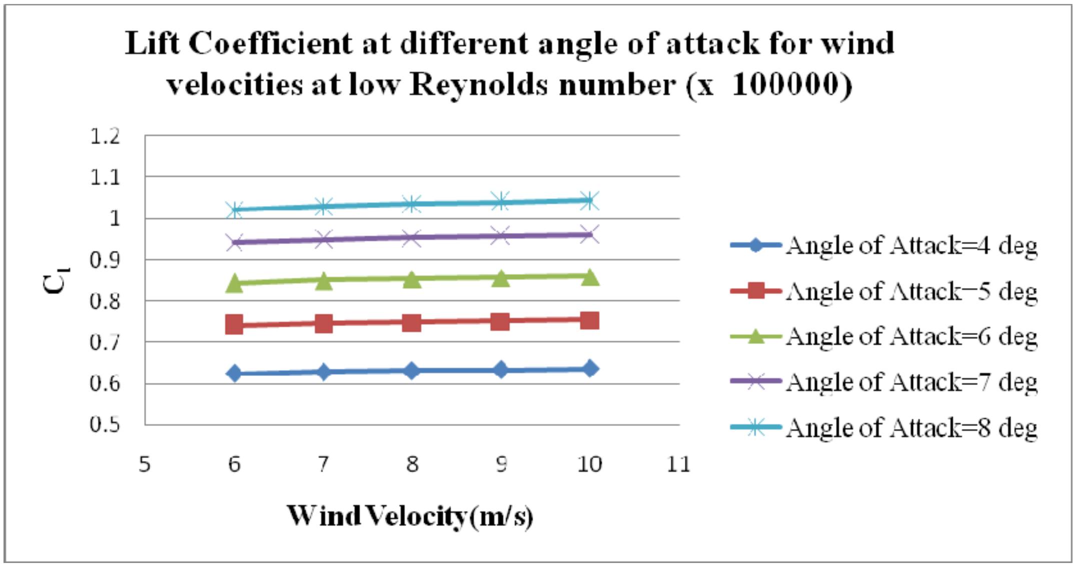

Figure 20: Lift Coefficient at different angle of attack for wind velocities at low Reynolds number (x100000)

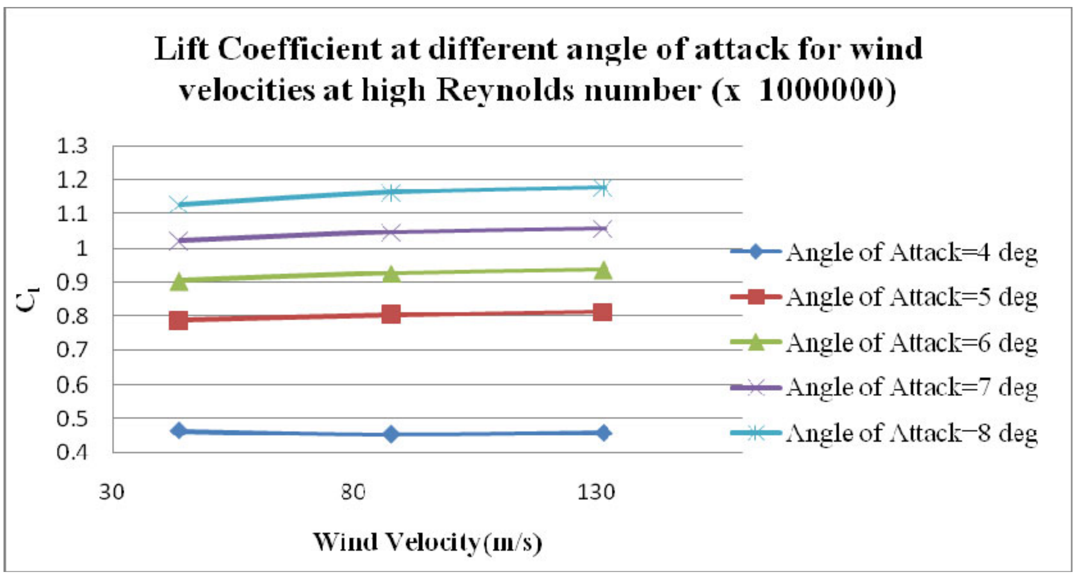

Figure 21: Lift Coefficient at different angle of attack for wind velocities at high Reynolds number (x1000000)

Combined effect of AOA and Wind velocity on Drag Coefficient at low Reynolds number and high Reynolds number

Figure 22 and figure 23 shows the Drag coefficient at different angle of attack for wind velocities at low Reynolds number and high Reynolds number respectively. The following are the observations from them:

a) The drag coefficient is increasing as the angle of attack is increased.
b) The drag coefficient is decreasing as the wind velocity is increased.
c) The difference in increase in drag coefficient at AOA 4^{o} to 5^{o} is more compared to other successive AOA at high Reynolds number.

d) The difference in decrease in drag coefficient is identical as the wind velocity increases.
e) The difference in increase in drag coefficient is identical as the angle of attack increases.

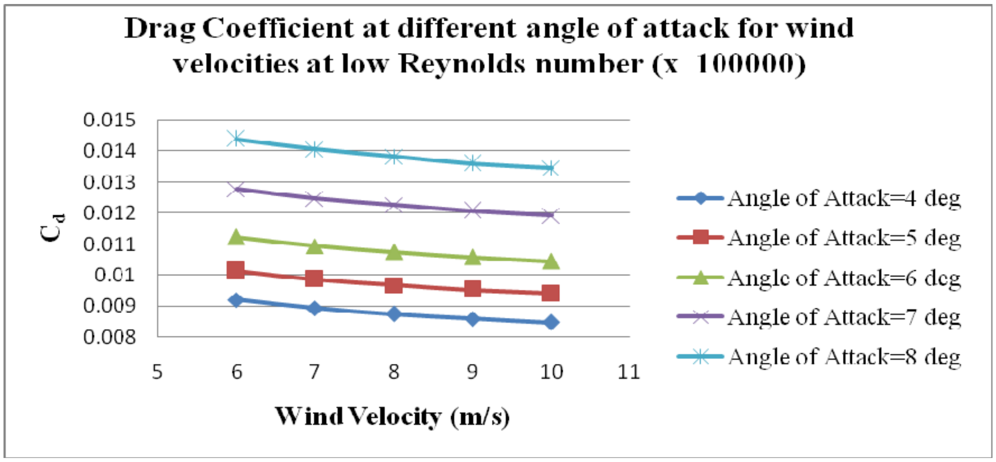

Figure 22: Drag Coefficient at different angle of attack for wind velocities at low Reynolds number (x100000)

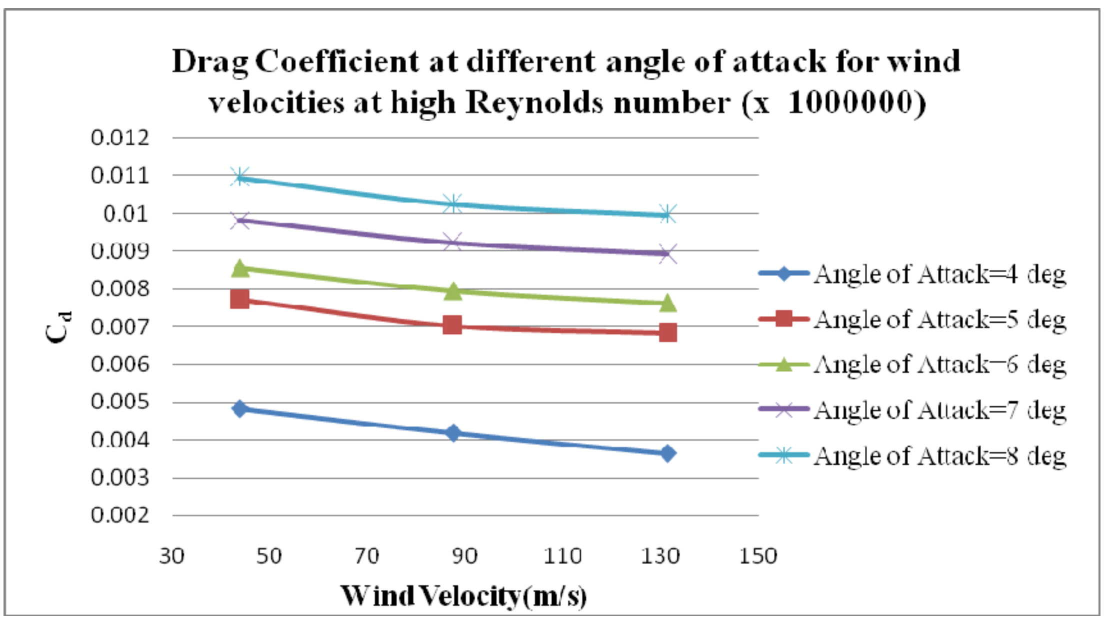

Figure 23: Drag Coefficient at different angle of attack for wind velocities at high Reynolds number (x1000000)

Combined effect of AOA and Wind velocity on Lift Coefficient to Drag Coefficient ratio (C_l/C_d) at low Reynolds number and high Reynolds number

Figure 24 and figure 25 shows the Lift coefficient to Drag coefficient ratio (C_l/C_d) at different angle of attack for wind velocities at low Reynolds number and high Reynolds number respectively. The following are the observations from them:

1. At angle of attack 4° to 8°, the lift coefficient to drag coefficient ratio (C_l/C_d) increases with increase in wind velocity.

2. The lift coefficient to drag coefficient ratio (C_l/C_d) increases with increase in angle of attack 4° to 6° and further decreases with increase in angle of attack.
3. At the angle of attack 6° the maximum C_l/C_d values are obtained at low Reynolds number and high Reynolds number.

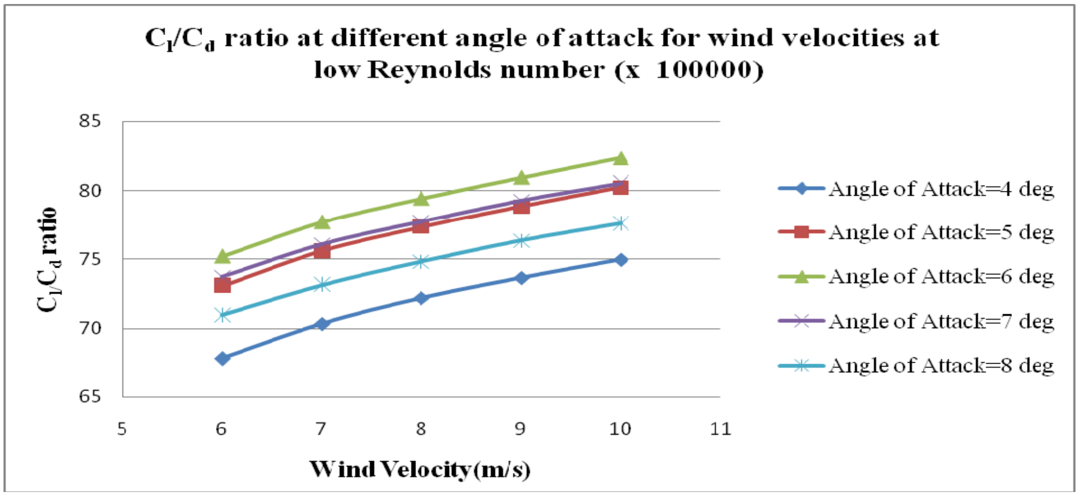

Figure 24: C_l/C_d ratio at different angle of attack for wind velocities at low Reynolds number ($x10^5$)

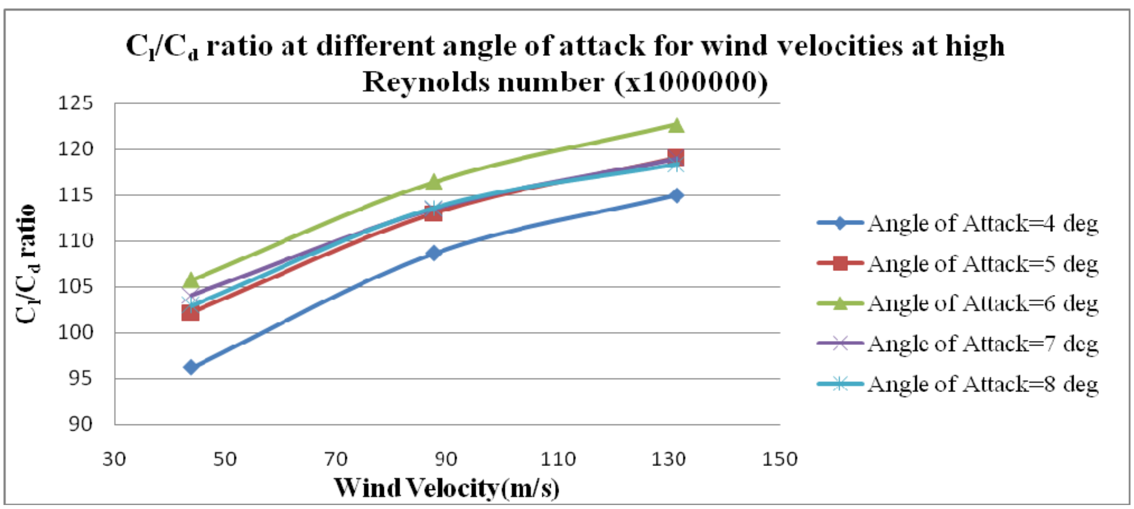

Figure 25: C_l/C_d ratio at different angle of attack for wind velocities at high Reynolds number ($x10^6$)

6. Conclusions

From the CFD results obtained, the following conclusions are made:

i. The increase in wind velocity increases the velocity of flow on the aerofoil.

ii. The increase in angle of attack 4° to 8° increases the velocity of flow on the aerofoil.

iii. Coefficient of lift (C_l) and coefficient of drag (C_d) have increased with the increase in the angle of attack

iv. For angle of attack 4^o to 8^o,Coefficient of lift (C_l) has increased as the Reynolds number is increased.

v. For angle of attack 4^o to 8^o, Coefficient of drag (C_d) has decreased as the Reynolds number is increased.

vi. For angle of attack 4^o to 8^o, the percentage increase in ratio coefficient of lift to coefficient of drag (C_l/C_d) decreases from 3.5% to 1.5% with increase in low values of Reynolds number.

vii. For angle of attack 4^o to 8^o, the percentage increase in ratio coefficient of lift to coefficient of drag (C_l/C_d) decreases from 11.5% to 4% with increase in high values of Reynolds number.

viii. The ratio of lift coefficient to drag coefficient (C_l/C_d) has increased with increase in angle of attack in the range 4^o to 6^o and has decreased with increase in angle of attack beyond 6^o.

ix. For low Reynolds Number study, at angle of attack 6^o, the maximum value of C_l/C_d=82.38 is observed at 10 m/s.

x. For high Reynolds Number study, at angle of attack 6^o, the maximum value of C_l/C_d=122.65 is observed at 131.5 m/s.

REFERENCES

1. Abbott I.H., Von Doenhoff A.E., Stivers L., NACA Report No. 824 – Summary of Airfoil Data, National Advisory Committee for Aeronautics, p 175; 1945.
2. C.A. Baxevanoua, P.K. Chaviaropoulosb, S.G. Voutsinas c, N.S. Vlachosa; Evaluation study of a Navier–Stokes CFD aeroelastic model of wind turbine airfoils in classical flutter; Journal of Wind Engineering and Industrial Aerodynamics;2008.
3. GiridharRamanujam, HüseyinÖzdemir and H. W. M. Hoeijmakers; Improving Airfoil Drag Prediction; American Institute of Aeronautics and Astronautics, Inc.; 2016.
4. Liu, X., Lu, C., Liang, S., Godbole, A., & Chen, Y. "Vibration-induced aerodynamic loads on large horizontal axis wind turbine blades". Applied Energy, 185, pp 1109–1119. 2017.
5. MingweiGe, De Tianand Ying Deng; Reynolds Number Effect on the Optimization of a Wind Turbine Blade for Maximum Aerodynamic Efficiency; Journal of Energy Engineering; 2016.
6. Muhammad FaizanYounas, Awais Ali and Muhammad DaudShafique;"CFD Simulation of HAWT Blade and Implementation of BEM Theory"; Sukkur IBA Journal of Emerging Technologies; Vol 2 No 2; 2019.
7. P. K. Nigam, NitinTenguria and M. K. Pradhan; Verification of Sliding Ratio (Cl/Cd) of Airfoil through CFD Analysis; Journal of Scientific Research; Volume 64, Issue 1, 2020.
8. P.K.Nigam, NitinTenguria and M.K.Pradhan; Analysis of horizontal axis wind turbine blade using CFD; InternationalJournalofEngineering,ScienceandTechnology Vol.9,No.2,2017pp.46-60.
9. Sayed M.A, Kandil H.A, ShaltotA."Aerodynamic analysis of different wind-turbine-blade profiles using finite-volume method" Energy Conversion and Management, Vol. 64pp.541-550, 2012.
10. UmeshChaudhary; Sisir Kumar Nayak; "Micro and small-scale HAWT blades airfoils study through CFD for low wind applications"; Annual IEEE India Conference (INDICON);2015.